J|A|C|S ARTICLES

Published on Web 09/25/2009

Ab Initio Nonadiabatic Molecular Dynamics of Wet-Electrons on the TiO_2 Surface

Sean A. Fischer,[†] Walter R. Duncan,[‡] and Oleg V. Prezhdo*,[†]

Department of Chemistry, University of Washington, Seattle, Washington 98195, and Schrodinger Inc., 101 SW Main Street, Suite 1300, Portland, Oregon 97204

Received August 4, 2009; E-mail: prezhdo@u.washington.edu

Abstract: The electron transfer (ET) dynamics of wet-electrons on a TiO_2 surface is investigated using state-of-the-art ab initio nonadiabatic (NA) molecular dynamics (MD). The simulations directly mimic the time-resolved experiments [*Science* **2005**, *308*, 1154] and reveal the nature of ET in the wet-electron system. Focusing on the partially hydroxylated TiO_2 surface with 1-monolayer water coverage, and including electronic evolution, phonon motions, and electron−phonon coupling, the simulations indicate that the ET is sub-10 fs, in agreement with the experiment. Despite the large role played by low frequency vibrational modes, the ET is fast due to the strong coupling between the TiO_2 surface and water. The average ET for the system has equal contributions from the adiabatic and NA mechanisms, even though a very broad range of individual ET events is seen in the simulated ensemble. Thermal phonon motions induce a large fluctuation of the wet-electron state energy, generate frequent crossings of the donor and acceptor states, and drive the adiabatic mechanism. The rapid phonon-assisted NA tunneling from the wet-electron state to the TiO_2 surface is facilitated by the strong water−TiO_2 electronic interaction. The motions of molecular water have a greater effect on the ET dynamics than the hydroxyl vibrations. The former contribute to both the wet-electron state energy and the water−TiO_2 electronic coupling, while the latter changes only the energy and not the coupling. Delocalized over both water and TiO_2, wet-electrons are supported by a new type of state that is created at the interface due to the strong water−TiO_2 interaction and that cannot exist separately in either material. Similar states are present in a number of other systems with strong interfacial coupling, including certain dye-sensitized semiconductors and metal−liquid interfaces. The ET dynamics involving such interfacial states share many universal features, such as an ultrashort time scale and weak-dependence on temperature, surface defects, and other system details.

1. Introduction

Interfacial electron transfer (ET) is of fundamental importance in a wide variety of disciplines, and a vast amount of research has been devoted to understanding its nature.[1−24] Of particular interest is ET at metal−oxide/aqueous interfaces, as it underpins many chemical and physical phenomena.[25] Theoretical modeling and understanding of interfaces composed of two qualitatively different species is challenging and intellectually stimulating. It is not obvious which concepts and theoretical tools should be used for description of molecules bound to bulk materials. On the one hand, molecules are best understood by chemists who operate with discrete sets of molecular orbitals and vibrational modes. On the other hand, the electron and phonon

[†] University of Washington.
[‡] Schrodinger Inc.

(1) Nitzan, A.; Ratner, M. A. *Science* **2003**, *300*, 1384.
(2) Oregan, B.; Grätzel, M. *Nature* **1991**, *353*, 737.
(3) Hagfeldt, A.; Grätzel, M. *Acc. Chem. Res.* **2000**, *33*, 269.
(4) Holman, M. W.; Liu, R.; Adams, D. M. *J. Am. Chem. Soc.* **2003**, *125*, 12649.
(5) Klare, J. E.; Tulevski, G. S.; Sugo, K.; de Picciotto, A.; White, K. A.; Nuckolls, C. *J. Am. Chem. Soc.* **2003**, *20*, 6030.
(6) Fan, F. F.; Yao, Y.; Cai, L.; Cheng, L.; Tour, J. M.; Bard, A. J. *J. Am. Chem. Soc.* **2004**, *126*, 4035.
(7) Zhu, X. Y. *J. Phys. Chem. B* **2004**, *108*, 8778.
(8) Asbury, J. B.; Hao, E. C.; Wang, Y. Q.; Ghosh, H. N.; Lian, T. Q. *J. Phys. Chem. B* **2001**, *105*, 4545.
(9) Anderson, N. A.; Lian, T. Q. *Annu. Rev. Phys. Chem.* **2005**, *56*, 491.
(10) Huber, R.; Moser, J. E.; Grätzel, M.; Wachtveitl, J. *J. Phys. Chem. B* **2002**, *106*, 6494.
(11) Nozik, A. J. *Physica E* **2002**, *14*, 115.
(12) Ramakrishna, S.; Willig, F.; May, V.; Knorr, A. *J. Phys. Chem. B* **2003**, *107*, 607.
(13) Kamat, P. V. *J. Phys. Chem. C* **2007**, *111*, 2834–2860.
(14) Kongkanand, A.; Tvrdy, K.; Takechi, K.; Kuno, M.; Kamat, P. V. *J. Am. Chem. Soc.* **2008**, *130*, 4007–4015.
(15) Martinson, A. B. F.; Hamann, T. W.; Pellin, M. J.; Hupp, J. T. *Chem.-Eur. J.* **2008**, *14*, 4458–4467.
(16) Stier, W.; Prezhdo, O. V. *J. Phys. Chem. B* **2002**, *106*, 8047.
(17) Rego, L. G. C.; Batista, V. S. *J. Am. Chem. Soc.* **2003**, *125*, 7989.
(18) Thoss, M.; Kondov, I.; Wang, H. B. *Chem. Phys.* **2004**, *304*, 169.
(19) Duncan, W. R.; Stier, W. M.; Prezhdo, O. V. *J. Am. Chem. Soc.* **2005**, *127*, 7941.
(20) Abuabara, S. G.; Rego, L. G. C.; Batista, V. S. *J. Am. Chem. Soc.* **2005**, *127*, 18234.
(21) Duncan, W. R.; Craig, C. F.; Prezhdo, O. V. *J. Am. Chem. Soc.* **2007**, *129*, 8528.
(22) Duncan, W. R.; Prezhdo, O. V. *Annu. Rev. Phys. Chem.* **2007**, *58*, 143.
(23) Prezhdo, O. V.; Duncan, W. R.; Prezhdo, V. V. *Acc. Chem. Res.* **2008**, *41*, 339–348.
(24) Duncan, W. R.; Prezhdo, O. V. *J. Am. Chem. Soc.* **2008**, *130*, 9756–9762.
(25) Brown, G. E.; Henrich, V. E.; Casey, W. H.; Clark, D. L.; Eggleston, C.; Felmy, A.; Goodman, D. W.; Grätzel, M.; Maciel, G.; McCarthy, M. I.; Nealson, K. H.; Sverjensky, D. A.; Toney, M. F.; Zachara, J. M. *Chem. Rev.* **1999**, *99*, 77–174.

structure of semiconductors and metals is represented by physicists with infinite bands of periodically replicated states, energy−momentum dispersion relationships, and reciprocal spaces. On the practical side, the interfacial ET plays key roles in many photoinduced chemical reactions involved with photoelectrolysis,[26] color photography,[27] and photocatalysis.[28] A detailed description of the interface is also necessary to fully comprehend the ET dynamics of metal−oxide systems for use in photovoltaics.[2,3] The ubiquitous nature of water makes understanding the dynamics associated with the movement of charge through water and across a water interface essential in many fields.

There has been considerable interest in the structural and dynamical aspects of electrons solvated in water and other liquids,[29−47] ever since their optical spectra were identified.[48,49] The majority of the research has been directed at bulk liquid water and intermediate to small water anion clusters. For liquid water, the widely accepted Kevan structure proposes that an excess electron is stabilized by six octahedrally coordinated water molecules, each of which points one H atom toward the electron.[50] Having such a configuration in the bulk suggests that an isolated water cluster could bind an excess electron to its surface. Experimental measurements[29−36] and theoretical calculations[38−47] have borne out this assumption and shown the existence of water clusters that stabilize electrons on their surfaces via "dangling" H atoms, that is, H atoms that do not participate in strong hydrogen bonding.

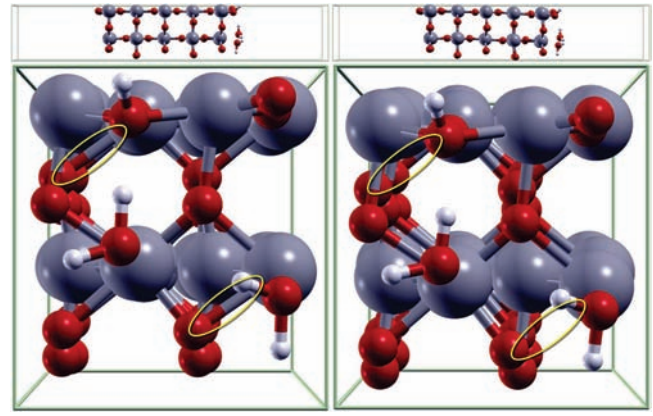

Figure 1. Side and surface views of the simulation cell showing the geometry of the wet-electron system optimized at 0 K (left) and during the molecular dynamics run at 100 K (right). Thermal fluctuations have a substantial impact on the system geometry, and hence its electronic structure. Compare the top panels and note the downward shift of the top layers of the TiO_2 slab (right) relative to the optimized geometry (left). Also, compare the bottom panels and note the missing Ti−O bonds in the upper left and lower right corners in the right panel taken from the dynamics run.

The dynamics of electrons at nonpolar-adsorbate/metal and polar-adsorbate/metal interfaces have also been studied.[51−54] These time-resolved experimental studies found that excited electrons are initially delocalized parallel to the interface. Within a few hundred femtoseconds, the electrons are partially stabilized by molecular rearrangements and become localized prior to relaxing back into the metal.

More recently, experimental and theoretical studies done on the H_2O/TiO_2 (110) interface have shown a short-lived state 2.4 ± 0.1 eV above the Fermi level. The electron in this state was localized on the surface and was partially hydrated by the water molecules. Hence, it was named the "wet-electron".[55,56] The femtosecond time-resolved two-photon photoemission (TR-2PP) study found that the wet-electron state was only observed on the reduced TiO_2 surface. Upon varying the surface coverage with water, a maximum in the signal intensity was found for 1 monolayer (ML) H_2O. 1 ML corresponds to one H_2O molecule adsorbed at every terminal five-coordinate Ti_{5c}^{4+} site; see Figure 1. The state lifetime was $\leq$15 fs. Static density functional theory (DFT) calculations were used to investigate the role of hydrogen bonding and the energy of the wet-electron state for the stoichiometric, partially reduced, and fully reduced TiO_2 (110) surfaces with varying coverages of water, ranging between 0 and 1 ML H_2O. The partially reduced surface involved bonding of one H atom at every other bridging oxygen on the TiO_2 substrate, creating 0.5 ML H. Respectively, the fully reduced surface had one H atom bonded to every bridging oxygen, that is, 1 ML H. The energy of the wet-electron state was found to decrease as the number of dangling H atoms on the surface was

(26) Jiang, D. L.; Zhao, H. J.; Zhang, S. Q.; John, R. *J. Catal.* **2004**, *223*, 212.
(27) Liu, D.; Hug, G. L.; Kamat, P. V. *J. Phys. Chem.* **1995**, *99*, 16768.
(28) Zhao, W.; Ma, W. H.; Chen, C. C.; Zhao, J. C.; Shuai, Z. G. *J. Am. Chem. Soc.* **2004**, *126*, 4782.
(29) Silva, C.; Walhout, P. K.; Yokoyama, K.; Barbara, P. F. *Phys. Rev. Lett.* **1998**, *80*, 1086.
(30) Coe, J. V.; Lee, G. H.; Eaton, J. G.; Arnold, S. T.; Sarkas, H. W.; Bowen, K. H.; Ludewigt, C.; Haberland, H.; Worsnop, D. R. *J. Chem. Phys.* **1990**, *92*, 3980.
(31) Kim, K. S.; Park, I.; Lee, S.; Cho, K.; Lee, J. Y.; Kim, J.; Joannopoulos, J. D. *Phys. Rev. Lett.* **1996**, *76*, 956.
(32) Byrd, J.; Chao, A.; Heifets, S.; Minty, M.; Raubenheimer, T. O.; Seeman, J.; Stupakov, G.; Thomson, J.; Zimmermann, F. *Phys. Rev. Lett.* **1997**, *79*, 79.
(33) Hammer, N. I.; Shin, J. W.; Headrick, J. M.; Diken, E. G.; Roscioli, J. R.; Weddle, G. H.; Johnson, M. A. *Science* **2004**, *306*, 675.
(34) Bragg, A. E.; Verlet, J. R. R.; Kammrath, A.; Cheshnovsky, O.; Neumark, D. M. *Science* **2004**, *306*, 669.
(35) Verlet, J. R. R.; Bragg, A. E.; Kammrath, A.; Cheshnovsky, O.; Neumark, D. M. *Science* **2005**, *307*, 93.
(36) Paik, D. H.; Lee, I.-R.; Yang, D.-S.; Baskin, J. S.; Zewail, A. H. *Science* **2004**, *306*, 672.
(37) Cramer, C. J.; Truhlar, D. G. *Acc. Chem. Res.* **2008**, *41*, 760–768.
(38) Schnitker, J.; Motakabbir, K.; Rossky, P. J.; Friesner, R. A. *Phys. Rev. Lett.* **1988**, *60*, 456.
(39) Wallqvist, A.; Martyna, G.; Berne, B. J. *J. Phys. Chem.* **1988**, *92*, 1721.
(40) Barnett, R. N.; Landman, U.; Cleveland, C. L.; Jortner, J. *J. Chem. Phys.* **1988**, *88*, 4429.
(41) Staib, A.; Borgis, D. *J. Chem. Phys.* **1995**, *103*, 2642.
(42) Prezhdo, O. V.; Rossky, P. J. *J. Chem. Phys.* **1997**, *107*, 5863.
(43) Prezhdo, O. V.; Rossky, P. J. *Phys. Rev. Lett.* **1998**, *81*, 5294.
(44) Boero, M.; Parrinello, M.; Terakura, K.; Ikeshoji, T.; Liew, C. C. *Phys. Rev. Lett.* **2003**, *81*, 226403.
(45) Jordan, K. D.; Wang, F. *Annu. Rev. Phys. Chem.* **2003**, *54*, 367.
(46) Shin, J. W.; Hammer, N. I.; Diken, E. G.; Johnson, M. A.; Walters, R. S.; Jaeger, T. D.; Duncan, M. A.; Christie, R. A.; Jordan, K. D. *Science* **2004**, *304*, 1137.
(47) Turi, L.; Sheu, W.-S.; Rossky, P. J. *Science* **2005**, *309*, 914.
(48) Hart, E. J.; Boag, J. W. *J. Am. Chem. Soc.* **1962**, *84*, 4090.
(49) Keene, J. P. *Nature* **1963**, *197*, 147.
(50) Kevan, L. *Acc. Chem. Res.* **1981**, *14*, 138.
(51) Ge, N.-H.; Wong, C. M.; Lingle, R. L., Jr.; McNeill, J. D.; Gaffney, K. J.; Harris, C. B. *Science* **1998**, *279*, 202.
(52) Miller, A. D.; Bezel, I.; Gaffney, K. J.; Garrett-Roe, S.; Liu, S. H.; Szymanski, P.; Harris, C. B. *Science* **2002**, *297*, 1163.
(53) Stähler, J.; Bovensiepen, U.; Meyer, M.; Wolf, M. *Chem. Soc. Rev.* **2008**, *37*, 2180.
(54) Bovensiepen, U.; Gahl, C.; Stähler, J.; Bockstedte, M.; Meyer, M.; Baletto, F.; Scandolo, S.; Zhu, X. Y.; Rubio, A.; Wolf, M. *J. Phys. Chem. C* **2009**, *113*, 979.
(55) Onda, K.; Li, B.; Zhao, J.; Jordan, K. D.; Yang, J. L.; Petek, H. *Science* **2005**, *308*, 1154–1158.
(56) Zhao, J.; Li, B.; Jordan, K. D.; Yang, J.; Petek, H. *Phys. Rev. B* **2006**, *73*, 195309.

increased, showing that these dangling H atoms play a crucial role in the stabilization of the electron. The partially reduced TiO_2 surface with 0.5 ML H and 1 ML H_2O was found to be the most relevant structure to the TR-2PP experiments of ref 55. A non-adiabatic (NA) ET mechanism was proposed to rationalize the experimental data.[57] While static DFT calculations have already provided a solid interpretation of the experiments, a comprehensive understanding of the time-resolved experimental data can be achieved only with a direct time-domain (TD) modeling of the ET process.

The present work uses NA molecular dynamics (MD) implemented within TDDFT[58] to characterize the photoinduced ET process in the wet-electron system. The NAMD simulation found ET occurring on a time scale that is consistent with the experimentally observed ultrafast decay of the wet-electron state. Both adiabatic and NA mechanisms contributed to ET. Surprisingly, despite the ultrafast time scale, the ET was driven primarily by bending motions of water molecules with intermediate frequencies around 1000 cm^{-1}. The fast OH stretching mode played only a minor role. One may expect that the results obtained with the wet-electron system are characteristic of the states that are delocalized across the interface due to strong electron donor−acceptor coupling. Similar states can be found at metal−liquid and molecule−semiconductor interfaces.

This Article is constructed as follows. The following section describes the key components of the theoretical approach together with the computational details of the NAMD simulation. The Results section starts by considering the geometric and electronic structure of the wet-electron system, which was both fully relaxed at 0 K and brought up to 100 K during an MD trajectory. The types of electronic states involved in the charge transport through the system are discussed. The role played by thermal phonon motions in creating an ensemble of initial conditions and driving the ET dynamics is fully explored. Finally, the electron injection events are investigated on the average, as seen in experiments, as well as within subpopulations of the initial conditions and at the level of individual ET events. This Article concludes with a summary of the most important findings.

2. Theory

The detailed description of the theoretical approach, which combines NAMD with TDDFT, can be found in refs 16, 19, 21, 24. The approach was used extensively to study the ET, relaxation, and delocalization dynamics in the alizarin−TiO_2 system.[19,21−24,58,59] Here, we start with the technical details beyond the now standard DFT and MD techniques applied to the wet-electron system, and then give a short description of the fundamental theory behind the TDDFT-NAMD method.

2.1. Simulation Details. In line with the previous experimental and theoretical studies of wet-electrons on the TiO_2 surface,[55−57,60] we have chosen a single surface of rutile TiO_2 (110). The distance between the five-coordinate Ti_{5c}^{4+} ions on this surface of TiO_2 allows for the formation of both molecule−surface and intermolecular hydrogen bonds, forming a stable first ML of H_2O.[57] Our simulation cell, shown in Figure 1, consists of 5 Ti layers of TiO_2 with the bottom two layers frozen in the bulk configuration. The most experimentally relevant interface structure[55] involves a partially reduced TiO_2 surface with 0.5 ML H and 1 ML H_2O. Therefore, one of the two bridging oxygen atoms present on the TiO_2 surface in the simulation cell has been reduced to a hydroxyl group, giving us 0.5 ML coverage of H. To achieve the 1 ML H_2O coverage, one water molecule is placed over every Ti_{5c}^{4+} ion. Periodic boundary conditions in three dimensions produce an array of slabs, and the vacuum seen to the left and right of the TiO_2 in the simulation cell in the top frames of Figure 1 ensures that the slabs do not interact with each other.

The electronic structure and adiabatic MD are obtained with the VASP code,[61] using a plane wave basis, the PBE density functional,[62,63] and the projector augmented wave (PAW) potentials.[64,65] After relaxing the geometry at 0 K, we used velocity rescaling to bring the temperature of the $H/H_2O/TiO_2$ system to 100 K, as in experiment.[55] We then carried out a 1 ps adiabatic MD simulation in the microcanonical ensemble with a 1 fs atomic time-step. The atomic trajectories from this adiabatic MD are used to sample initial conditions and perform the NAMD calculations, which are described below.

2.2. Nonadiabatic Molecular Dynamics with Time-Domain Density Functional Theory. We describe the NA effects in the ET dynamics by TDDFT within the Kohn−Sham (KS) approach.[16,19,21] The electron density of the system, $\rho(\mathbf{r}, t)$, which is the central quantity in DFT, is expressed within the KS approach by a sum of the densities of the occupied KS orbitals, $\varphi_p(\mathbf{r}, t)$. Application of the variational principle to the KS energy gives the evolution of the electronic density and produces a set of single-particle equations for the evolution of the KS orbitals:

$$i\hbar\frac{\partial\varphi_p(\mathbf{r},t)}{\partial t} = H(\mathbf{r},\mathbf{R},t)\varphi_p(\mathbf{r},t) \quad (1)$$

where $p = 1, 2, ..., N_e$, and N_e is the number of electrons. The Hamiltonian is time-dependent through the external potential created by the motion of the atoms. Dependence of the Hamiltonian on the electron density couples the single-particle equations.

We express the TD one-electron wave functions $\varphi_p(\mathbf{r}, t)$ in the adiabatic KS basis $\tilde{\varphi}_k(\mathbf{r}; \mathbf{R}(t))$, which is calculated with time-independent DFT, using the atomic positions from the adiabatic MD, described above. The focus is on the evolution of the orbital φ_{PE} occupied by the photoexcited (PE) electron. As argued previously,[19] the transfer dynamics are well represented by the evolution of the PE electron, which involves unoccupied molecular orbitals and TiO_2 conduction band (CB) states. All other electrons and orbitals are significantly separated in energy from the PE electron. The inclusion of the other states is only necessary when the longer time dynamics associated with the electron relaxation to the ground state are of interest.[21] The TDKS orbital that is occupied by the PE electron is expanded in the adiabatic KS basis covering the relevant energy range:

(57) Zhao, J.; Li, B.; Onda, K.; Feng, M.; Petek, H. *Chem. Rev.* **2006**, *106*, 4402–4427.
(58) Craig, C. F.; Duncan, W. R.; Prezhdo, O. V. *Phys. Rev. Lett.* **2005**, *95*, 163001.
(59) Duncan, W. R.; Prezhdo, O. V. *J. Phys. Chem. B* **2005**, *109*, 17998.
(60) Koitaya, T.; Nakamura, H.; Yamashita, K. *J. Phys. Chem. C* **2009**, *113*, 7236.
(61) Kresse, G.; Furthmüller, J. *Comput. Mater. Sci.* **1996**, *6*, 15.
(62) Perdew, J. P.; Burke, K.; Ernzerhof, M. *Phys. Rev. Lett.* **1996**, *77*, 3865.
(63) Perdew, J. P.; Burke, K.; Ernzerhof, M. *Phys. Rev. Lett.* **1997**, *78*, 1396.
(64) Kresse, G.; Joubert, D. *Phys. Rev. B* **1999**, *59*, 1758.
(65) Blöchl, P. E. *Phys. Rev. B* **1994**, *50*, 17953.

$$\varphi_{PE}(\mathbf{r}, t) = \sum_k c_k(t)\tilde{\varphi}_k(\mathbf{r};\mathbf{R}(t)) \quad (2)$$

By inserting this expansion into eq 1, we obtain the equation describing the evolution of the adiabatic state coefficients:

$$i\hbar\frac{\partial}{\partial t}c_j(t) = \sum_k c_k(t)(\varepsilon_k\delta_{jk} + d_{jk}) \quad (3)$$

where ε_k is the energy of the adiabatic state k, and d_{jk} is the NA coupling between KS orbitals k and j. The latter is given by

$$d_{jk} = -i\hbar\langle\tilde{\varphi}_j|\nabla_{\mathbf{R}}|\tilde{\varphi}_k\rangle\cdot\frac{d\mathbf{R}}{dt} = -i\hbar\left\langle\tilde{\varphi}_j\left|\frac{\partial}{\partial t}\right|\tilde{\varphi}_k\right\rangle \quad (4)$$

The extent of ET from the water layer to the TiO_2 surface is computed by integrating the electron density over the region of the simulation cell occupied by the waters and hydroxyl groups, Figure 1.

$$\int_{water}\rho_{PE}(\mathbf{r}, t)\,d\mathbf{r} = \int_{water}|\varphi_{PE}(\mathbf{r}, t)|^2 d\mathbf{r} = \sum_{k,j} c_k^*(t)c_j(t)\int_{water}\tilde{\varphi}_k^*(\mathbf{r}, \mathbf{R}(t))\tilde{\varphi}_j(\mathbf{r}, \mathbf{R}(t))\,d\mathbf{r} \quad (5)$$

Taking the time-derivative of eq 5 gives expressions for the adiabatic and NA contributions to the ET:[16]

$$\frac{d\int_{water}\rho_{PE}(\mathbf{r}, t)\,d\mathbf{r}}{dt} = \sum_{k,j}\left\{\frac{d(c_k^*c_j)}{dt}\int_{water}\tilde{\varphi}_k^*\tilde{\varphi}_j\,d\mathbf{r} + c_k^*c_j\frac{d\int_{water}\tilde{\varphi}_k^*\tilde{\varphi}_j\,d\mathbf{r}}{dt}\right\} \quad (6)$$

The change in the electron density described by the first term above originates from changing state occupations for fixed state localizations. The electronic transitions leading to the changes in the state occupations produce NA ET. The second term has fixed occupations of adiabatic states. The ET described by the second term arises due to changes in the localizations of the adiabatic states from the water layer to the TiO_2 surface. The localizations change when the system passes over a transition state generated by an avoided crossing of the adiabatic states. Hence, the second term corresponds to adiabatic ET. Note that even adiabatic ET can and does involve NA dynamics. To be transferred, the PE-electron in the water layer has to find a strongly coupled TiO_2 surface state by hopping over several uncoupled TiO_2 bulk states. The above definition of the NA transfer mechanism includes this factor by automatically considering contributions only from those NA transitions that produce the overall shift of the electron density from the water ML onto the metal−oxide. This is reflected in the integral over the water region, $\int_{water} d\mathbf{r}$.

The wet-electron state is identified in the simulation by finding the adiabatic state with the highest localization on the water/hydroxyl layer, left panel in Figure 2. The state is chosen within the energy range corresponding to the experimental measurements.[55] A similar approach was taken in the previous static DFT calculations,[56] which used a different DFT functional. Such state-selection procedure gives excellent agreement with the experiment. The state energy fluctuates around 2.6 eV above the Fermi energy, top panel in Figure 3. This is very close to the experimentally determined energy range of 2.4 ± 0.1 eV. The localization of the wet-electron state on the water layer

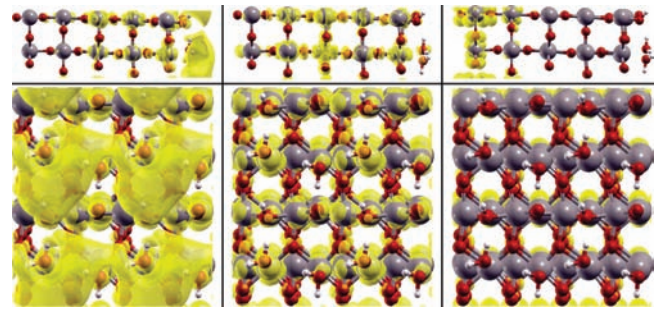

Figure 2. Charge densities for the wet-electron state (left), the surface state (middle), and the bulk state (right) of the wet-electron system. Charge is transferred sequentially from the wet-electron state through the surface state to the bulk state. Note the large delocalization of charge around the water molecules in the wet-electron state, which is due to the dangling H atoms that help stabilize the electron.

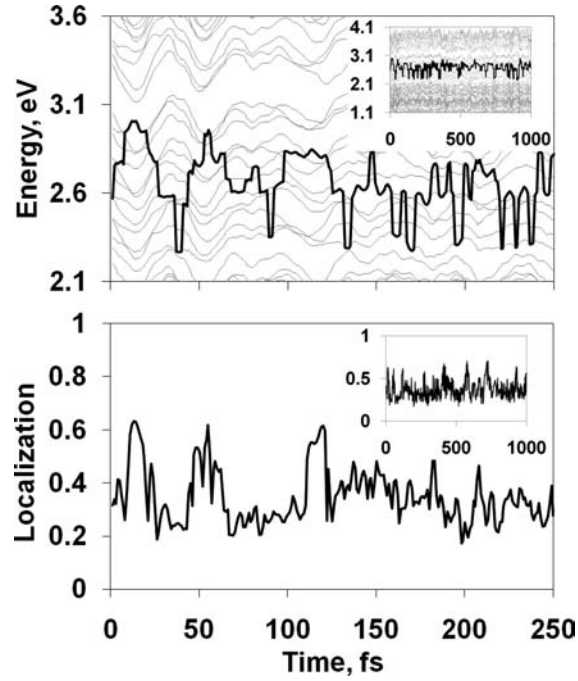

Figure 3. Top: Evolution of the wet-electron state energy (thick line) relative to the TiO_2 conduction band states. Fluctuations of about 0.5 eV result from atomic motions. Bottom: Evolution of the wet-electron state localization on the water monolayer. The wet-electron state has substantial localization on the TiO_2 substrate. Insets show the evolution of the energy and localization for a longer time.

fluctuates around 0.4, bottom panel in Figure 3. The wet-electron is significantly delocalized into the TiO_2 surface, left panel in Figure 2, due to the extremely strong water−TiO_2 electronic coupling. All other adiabatic states within the relevant energy range, top panel of Figure 3, have noticeably lower localizations on the water layer.

To simulate the ET dynamics, we first randomly select an initial system geometry from the 1 ps adiabatic MD run. The wet-electron state is selected as described above. The electron is promoted from the Fermi level to this state. The energies and the NA couplings between the wet-electron and TiO_2 states within the relevant energy range are computed. The PE-electron is propagated by solving eq 5 using the second-order differencing scheme and a 10^{-3} fs time-step. The average behavior of the system is determined by sampling hundreds of initial conditions from the MD trajectory.

3. Results

Time-domain modeling of the wet-electron system has provided a detailed picture of the ET process. Thermal fluctuations of the atoms play a key role in the electronic dynamics by modulating the wet-electron state energy and drive the system through regions of strong donor−acceptor coupling. The transfer occurs from a PE state that is substantially localized on the TiO_2 substrate to begin with, and, on the time scale of the ET, both adiabatic and NA mechanisms compete. In this section, we describe and analyze the results of our ab initio studies.

3.1. Geometry and Electronic Structure of the Wet-Electron System. The structure of the system studied presently was chosen to approximate that used in the TR-2PP experiments of ref 55, as explained earlier in this Article. Figure 1 shows both the minimum energy geometry at 0 K (left frame) and an example of the geometry during the MD run at 100 K (right frame). Thermal motions can have an impact on the structure of the system. In the minimum energy geometry, the Ti atoms in the TiO_2 substrate form two straight rows, while in the geometry from the dynamics run, the slab has shifted relative to the two Ti layers that are frozen in the bulk configuration; compare the top frames in Figure 1. Various angles and bond lengths involving the Ti and O atoms vary: compare the bottom panels showing the surface view, and note the missing Ti−O bonds in the upper left and lower right corners in the right panel taken from the dynamics run, as highlighted by the ovals. At the same time, the location and orientation of the water molecules and hydroxide groups change very little during the 1 ps simulation time. One of the two H atoms of each water molecule is strongly hydrogen bonded to the bridging O atoms of the TiO_2 surface. The other H atom sits on top of Ti atoms and points slightly away from the surface, similarly to the hydroxyl H atom. The hydroxyl H atom together with the non-hydrogen bonded H atoms of the water molecules provide the Coulomb stabilization of the wet-electron state, Figure 2.

Figure 2 shows the spatial distribution of the charge density for three different types of states of the wet-electron system. In the left frame is the wet-electron state. This state is significantly delocalized between the H/H_2O solvent layer and the first three layers of the TiO_2 surface. The network of hydrogen bonds on the surface of the TiO_2 is what determines the spatial distribution of charge for the wet-electron state. The strong hydrogen bonds formed between one of the H atoms of the surface water molecules and the bridging O atoms prevent these H atoms from stabilizing an excess electron that is injected into the water ML. On the other hand, there is only a weak interaction between the other H atom and the O atom of the adjacent water molecule. Also, there is a very weak interaction between the H atom of the surface hydroxyl group and the O atom of the adjacent water molecule. These weak interactions are the result of the physical distance between the involved species and the fact that the other atoms bound to the involved species are participating in stronger interactions. As can be seen from Figure 2, the weak hydrogen bonds allow the dangling H atoms to stabilize the excess electron. The arrangement of the dangling H atoms is such that a large delocalization of the charge density results. The other frames in Figure 2 show a state that is delocalized over the middle of the simulation cell as well as a state localized on the cell side opposite to the H/H_2O layer. The charge moves through the system by going sequentially from the wet-electron state through the surface to the bulk. The movement of charge through the system is the result of atomic motions.

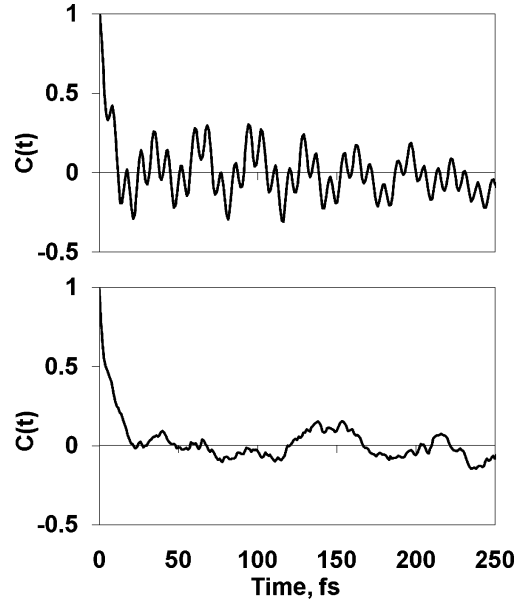

Figure 4. Autocorrelation functions (ACF) of the energy (top) and localization (bottom) of the wet-electron state shown in Figure 3. Both the energy and the localization ACFs decay on the same time scale; however, the energy ACF shows more sustained correlation with a high frequency. The localization ACF shows a low frequency oscillation much closer to zero.

3.2. Thermal Fluctuations. The motion of the atoms is the driving force behind ET. It generates the NA coupling that causes change in the occupations of the adiabatic states and drives NA ET, eq 6. Atomic motions shift the wet-electron state density between different adiabatic states, resulting in adiabatic ET. The top frame of Figure 3 shows the evolution of the wet-electron state energy relative to the CB states of TiO_2. The calculated average energy of the wet-electron state is ∼2.6 eV above the Fermi level, in good agreement with the energy of the wet-electron state observed in ref 55. Significant fluctuations of the wet-electron state energy of approximately 0.5 eV are due to the thermal motion of the atoms. It can be seen in Figure 3 that the wet-electron state crosses many of the TiO_2 CB states; this multitude of crossings can lead to efficient adiabatic ET. A crossing of strongly coupled wet-electron and TiO_2 surface state generates a transition state for adiabatic ET. Atomic motion also contributes to the NA mechanism, as the NA coupling is directly proportional to the velocity of the atoms, eq 6.

The evolution of the localization of the wet-electron state is shown in the bottom frame of Figure 3. In the figure, the *y*-axis gives the fraction of the wet-electron state density that exists on the water molecules and hydroxyl groups. The wet-electron state localization spreads across the H/H_2O MLs and into the TiO_2 substrate. In fact, the TiO_2 substrate supports much of the wet-electron state: on the average, less than 50% of the wet-electron state is localized within the solvent layer. Examples can be found in which the solvent layer localization exceeds 60% and drops as low as 20%. This spread in the localization between the adsorbant and the substrate is due to the strong electronic coupling between the two subsystems. It can be seen clearly in Figure 2 where the spatial density of the charge for the wet-electron state reaches all of the way to the lower layers of the TiO_2 substrate in the simulation cell.

The autocorrelation functions (ACFs) shown in Figure 4 quantify the time correlations in the fluctuations of the wet-electron state energy and localization. Both the energy and the

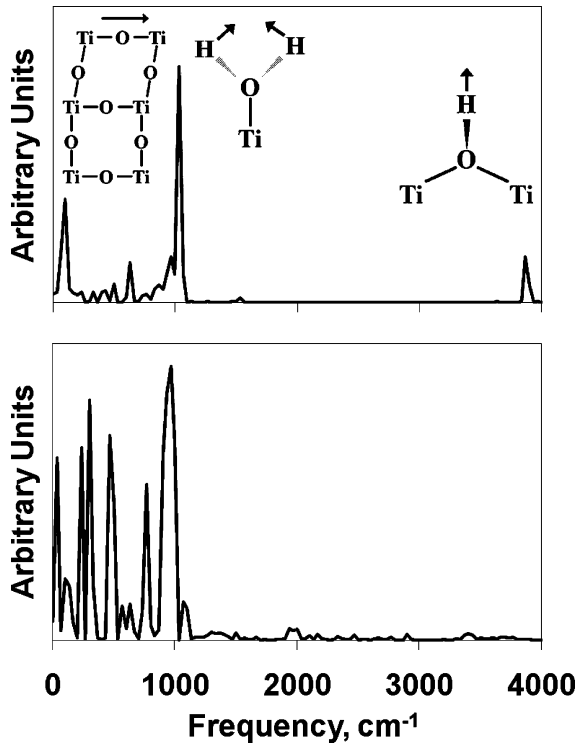

Figure 5. Fourier transforms (FT) of the energy (top) and localization (bottom) of the wet-electron state evolutions shown in Figure 3. The diagrams illustrate the atomic motions that are responsible for the FT peaks: the 3800 cm^{-1} peak is due to a combined wagging and stretching motion of the surface hydroxide, the peak at 1000 cm^{-1} is due to a bending motion of the H_2O molecules on the surface, and the low frequency modes are due to side movement of the TiO_2 surface, which can be seen most clearly in the side views of the simulations cells in Figure 1. The localization FT is dominated by a wide range of low frequency modes.

localization ACFs, top and bottom frames of Figure 4, respectively, show a rapid initial decay on approximately the same time scale. This is a reflection of a poorly correlated, random thermal motion of the atoms, involving multiple vibrational modes over a broad frequency range. This is not surprising, because the wet-electron state is delocalized over both the rapidly moving H/H_2O layer and the slow TiO_2, Figure 2. Most of the initial memory of the wet-electron state energy and localization is lost within 30 fs. After the rapid initial decay, the energy ACF oscillates at a high frequency. This oscillatory behavior suggests that evolution of the wet-electron state energy is not completely random, but is modulated by periodic vibrations of part of the system. The localization ACF also shows an oscillation after the initial decay, but its oscillation is of a much lower frequency with less amplitude. Thus, the evolution of the localization is also not completely random and also modulated by periodic vibrations, but of a different part of the system.

To elucidate the atomic motions that drive the evolution of the wet-electron, we computed Fourier transforms (FTs), Figure 5, of the energy and localization data from Figure 3. The FTs support the conclusions drawn directly from the ACFs, Figure 4. The FT of the energy evolution, top frame of Figure 5, has the majority of peaks in the low frequency region but also has a small contribution from a mode at ~3800 cm^{-1}. That peak is due to the stretching motion of the surface hydroxyl group, as illustrated by the insert cartoon. The peak at ~1000 cm^{-1} is the result of the bending motion of the surface water molecules, while the low frequency peak is attributed to the mass motion of the TiO_2 perpendicular to the long axis of the simulation cell; also see Figure 1. A number of peaks between 200 and 800 cm^{-1} correspond to librational, that is, restricted rotational, motions of water molecules. Shown in the bottom frame of Figure 5, the localization FT is dominated by low frequency vibrational modes and has no significant peaks beyond 1000 cm^{-1}.

A priori, one may expect that the wet-electron state properties should depend on the high frequency OH motions, because the wet-electron is supported by the H/H_2O layer. This is true for the state energy, but not localization. Changes in the OH bond distance with the 3800 cm^{-1} stretch frequency affect the energy of the orbital localized on this bond. The electron is stabilized by the network of hydrogen bonds, and high frequency motions of this network impact the electron energy. At the same time, these motions do not affect the localization of the state, because they can produce a rearrangement of the spatial charge density on the surface, but are not likely to push the charge density down into TiO_2. In contrast, bending of the polar OH bonds at frequencies around 1000 cm^{-1} changes the electrostatic interaction between the surface and the adsorbed ML and causes a redistribution of the wet-electron density between the ML and the surface. Water librations at frequencies between 200 and 800 cm^{-1} also affect the wet-electron properties, particularly its localization. Librations allow the hydrogen atoms to turn into and out of the regions of high charge density. The very low frequency mass movement of the Ti and O atoms of the substrate influences both energy and localization of the wet-electron state. The energy is affected because the wet-electron state extends significantly into TiO_2. The localization is affected because these motions can increase separation between the Ti and O atoms; see top left and bottom right corners of the surface view of the geometry in the right frame of Figure 1. The increased Ti−O separation allows the Ti atoms to assume a more electrophilic character and to draw the wet-electron density into the semiconductor. A similar Ti−O bond dilation is responsible for the defect charge stabilization in reduced TiO_2, as discussed by Minato et al.[66] The strong influence of the low frequency vibrational modes on the evolution of the PE state energy and localization was observed also in our previous study of the alizarin−TiO_2 system,[19] where the majority of peaks occurred at frequencies less than 1000 cm^{-1}. In both alizarin−TiO_2 and wet-electron systems, the ultrafast ET is driven by low frequency modes. This rather surprising fact is rationalized by the high density of acceptor states and strong electron donor−acceptor coupling. Even a slight motion of atoms results in energy crossings between the wet-electron and acceptor states. Most of such crossings give ET, because the donor−acceptor coupling is very strong: water molecules directly interact with TiO_2. A small fraction of the vibrational period of a slow mode is sufficient to generate the state crossings and to produce the ultrafast ET.

The wet-ET at the hydrated TiO_2 interface is so fast that the photoinduced change in the electronic density is not given sufficient time to alter the geometric structure of the system relative to the ground state. The nature of the atomic motion remains thermal. In contrast, wet-electrons at the TiO_2/methanol interface live significantly longer than in the aqueous system.[67]

(66) Minato, T.; Sainoo, Y.; Kim, Y.; Kato, H. S.; Aika, K.-I.; Kawai, M.; Zhao, J.; Petek, H.; Huang, T.; He, W.; Wang, B.; Wang, Z.; Zhao, Y.; Yang, J.; Hou, J. G. *J. Chem. Phys.* **2009**, *130*, 124502.
(67) Li, B.; Zhao, J.; Onda, K.; Jordan, K. D.; Yang, J. L.; Petek, H. *Science* **2006**, *311*, 1436–1440.

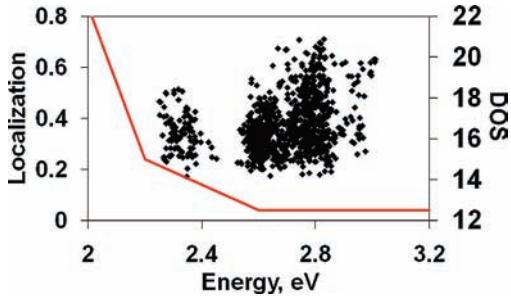

Figure 6. Localization of the wet-electron state on the H/H_2O layer (◆) and TiO_2 DOS (red line) as functions of energy. The DOS is given in number of states per eV per simulation cell. The localization varies significantly over a short energy range. There exists a small subdistribution at a lower energy, corresponding to the lower turning point of the energy fluctuation in the top frame of Figure 3 and associated with the bending motions of the H_2O molecules. The TiO_2 DOS is lower at higher energies in this range, accounting for the higher localization of the wet-electron state on the H/H_2O layer that is seen at higher energies, Figure 3.

As a result, the ET becomes strongly coupled to a proton motion, resulting in a proton-coupled ET (PCET). PCET is more complex than ET.[68−70] It may require an explicit quantum-mechanical treatment of both electron and proton.[71,72]

3.3. Distribution of Wet-Electron States. The motion of the atoms creates a distribution of wet-electron state energies and localizations. Different members of this ensemble produce starting points for the ET process. Over the course of the dynamics run, the localization of the wet-electron state on the surface MLs does not appear to track the fluctuations in the state energy very closely. However, comparing the top and bottom frames of Figure 3, one can see a moderate correlation, in which higher levels of localization on the surface MLs are achieved for higher wet-electron state energies, when the state is pushed up further into the CB of TiO_2. This correlation may appear surprising at first, because one expects increased wet-electron state delocalization with higher density of TiO_2 states, and the density of states (DOS) generally grows with energy. The explanation resides in the fact that the wet-electron state is already in the region of high TiO_2 DOS and that the DOS in this energy region fluctuates as a function of energy. In particular, the DOS is somewhat smaller where the wet-electron state energy is higher, as can be seen in Figure 6. This unusual energy dependence of the TiO_2 DOS is associated with the $t_{2g}-e_g$ splitting of the CB. It has been investigated experimentally by the inverse photoemission spectroscopy.[73]

A consequence of this fluctuation in the TiO_2 DOS is that two distinct subdistributions developed from the MD run, shown in Figure 6. The majority of the wet-electron states lie within 2.55−2.95 eV above the Fermi energy with localization on the H/H_2O layer ranging from 20% to 70%. A distinct subdistribution exists at energies from 2.25 to 2.45 eV. This smaller part of the ensemble of the wet-electron states is more significantly delocalized into the TiO_2 surface, with the water layer localization rarely exceeding 50%. The origin of the bimodal distribution can be traced to the fluctuation of the wet-electron state energy shown in the top frame of Figure 3. The two subdistributions correspond to the two turning points in the energy oscillation. The presence of the lower energy subdistribution is caused by the fact that the localization of the wet-electron state on the H/H_2O MLs is generally low. This makes it more likely that there will be another state of similar localization that exists at a slightly lower energy and that atom fluctuations cause a small degree of switching between these states. In line with the slight difference in the energy and localization for the two subdistributions, there is a slight difference in the ET dynamics origination from these two subsets of initial conditions, as is analyzed below.

The ET dynamics simulation was performed assuming that the initial photoexcitation promotes the system into an eigenstate of the electronic Hamiltonian, for example, into an adiabatic state. This is the most common assumption made in spectroscopic studies. It is rigorously valid if the system is excited by a continuous wave radiation. The experiments reported in ref 55 used a short laser pulse, which excites the system into a superposition of adiabatic states, whose energy width is determined by the inhomogeneous broadening and the time-energy uncertainty principle. The laser pulse of duration 10 fs has the energy range of about 0.06 eV. This energy range is smaller than the distribution of the wet-electron state energies shown in Figure 6. Therefore, different parts of the inhomogeneous distribution of the wet-electron states, and the low and high energy subdistributions in particular, can be excited selectively in the experiment.

3.4. Electron Transfer Dynamics. The strong coupling between the H/H_2O ML and the TiO_2 surface, together with the high density of TiO_2 states at the wet-electron state energy, create favorable conditions for the ultrafast ET. These two factors are also responsible for the large delocalization of the wet-electron between the adsorbant and the surface, such that the ET process starts from a state with an already significant contribution from TiO_2. Only a fraction of the charge remains to be transferred from the water to the surface. The simulation indicates that, in addition to the wet-electron state, a distinct type of states localized within the surface exists in the system, Figure 2. Hence, the electron evolution from the TiO_2 surface into the bulk can be considered as a separate step that follows the wet-electron transfer step. On the time scale of the ET, both adiabatic and NA mechanisms compete. Adiabatic ET occurs at crossings between the wet-electron and TiO_2 CB state energies and involves a change in the localization of the occupied adiabatic state from the donor to the acceptor. Nonadiabatic ET involves direct tunneling or hopping between the wet-electron and TiO_2 states. It does not require a state crossing, although the tunneling barrier in space domain, or the hopping gap in energy domain, is smaller around a crossing region. Both mechanisms are accounted for in our simulations and are distinguished from each other via eq 6.

Figure 7 presents the dynamics of the ET process for the wet-electron system. The top frame shows the average behavior of the total (solid line), adiabatic (dashed line), and NA (dotted line) ET. The transfer occurs in ∼7 fs and has essentially equal contribution from the adiabatic and NA mechanisms. The ET coordinate for the total ET starts at approximately 0.6, indicating that roughly 60% of the wet-electron state is localized on the TiO_2 to start. This high localization of the state on the TiO_2 at

(68) Isborn, C.; Hrovat, D. A.; Borden, W. T.; Mayer, J. M.; Carpenter, B. K. *J. Am. Chem. Soc.* **2005**, *127*, 5794–5795.
(69) Headrick, J. M.; Diken, E. G.; Walters, R. S.; Hammer, N. I.; Christie, R. A.; Cui, J.; Myshakin, E. M.; Duncan, M. A.; Johnson, M. A.; Jordan, K. D. *Science* **2005**, *308*, 1765–1769.
(70) Roscioli, J. R.; McCunn, L. R.; Johnson, M. A. *Science* **2007**, *316*, 249–254.
(71) Chakraborty, A.; Pak, M. V.; Hammes-Schiffer, S. *Phys. Rev. Lett.* **2008**, *101*, 153001.
(72) Chakraborty, A.; Pak, M. V.; Hammes-Schiffer, S. *J. Chem. Phys.* **2008**, *129*, 014101.
(73) See, A. K.; Thayer, M.; Bartynski, R. A. *Phys. Rev. B* **1993**, *47*, 13722.

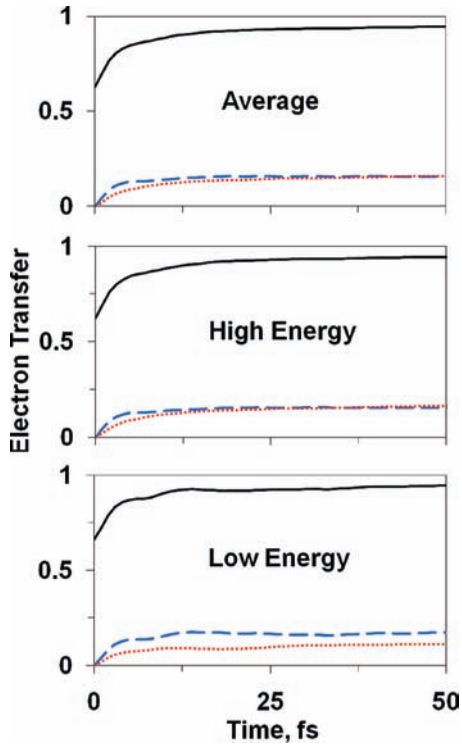

Figure 7. Average electron transfer (ET) dynamics (top), ET from the high energy distribution (middle), and ET from the low energy distribution (bottom) shown in Figure 6. In all plots, the solid black line is the total ET, the dashed blue line is the adiabatic contribution, and the dotted red line is the NA contribution. Note that the total ET starts around 0.6, indicating that much of the charge density of the wet-electron state is already localized on the TiO_2; see bottom frame of Figure 3 and Figure 6. The average ET and ET from the high energy distribution contain equal contributions of the adiabatic and NA ET mechanisms. The low energy distribution leads to a greater adiabatic ET contribution, because low energy electrons rapidly move up in energy and cross many TiO_2 states; see top frame of Figure 3.

the beginning is conducive to fast ET, as this indicates strong coupling between the wet-electron and the TiO_2 states.

The middle and bottom frames of Figure 7 show the ET dynamics averaged over the high and low energy distributions seen in Figure 6. The time scale of the transfer is the same for each distribution as for the total average ET. The high energy distribution's ET dynamics are almost identical to the total average dynamics of the system, which is expected considering the size of that distribution relative to the low energy one. Dynamics for the low energy distribution, however, have a larger contribution from the adiabatic mechanism. This is because the low energy distribution experiences more crossings with TiO_2 CB states; see Figure 3, which is favorable for adiabatic ET.

The ET dynamics averaged over all NAMD runs paints a straightforward picture of the behavior of the system; however, the individual ET events can be quite complex and varied. Figure 8 illustrates this with examples of individual ET events from a collection of random initial conditions. The top left of Figure 8 shows an example that is very similar to the average behavior, albeit with more adiabatic than NA character. The top right frame demonstrates the complexity that is possible. There are multiple movements of the electron back and forth before it begins to settle in TiO_2. The forward and back-ET movements are associated with fast repeated crossings between the wet-electron state and surface states that are strongly coupled to it. Beyond the simplicity or complexity of the transfer event, the adiabatic and NA character of an individual event can vary

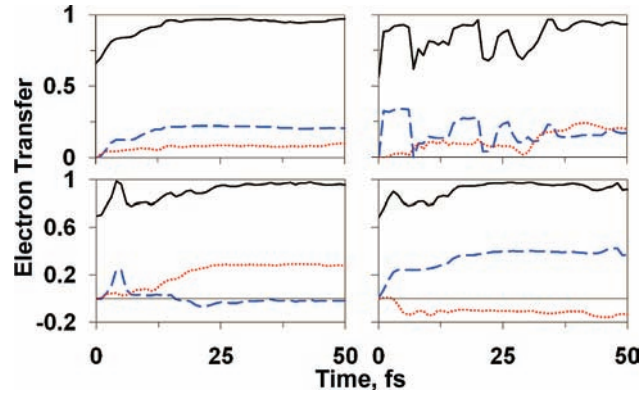

Figure 8. Examples of individual ET events. The lines are the same as in Figure 6. The upper left frame displays a simple example where the individual transfer is similar to the average. The upper right frame illustrates a rapid sequence of forward and backward adiabatic ET events. The lower left frame shows an initial adiabatic transfer and back transfer followed by a sustained NA ET. The lower right frame displays a predominantly adiabatic ET accompanied by a moderate NA transfer back into the wet-electron state.

widely. In the bottom left of Figure 8 is an example of a transfer event that starts as an adiabatic transition of wet-electron into a TiO_2 surface state. Rapidly, the surface state transitions the elctron back onto the water and hydroxyl molecules. The NA mechanisms then take over and complete the ET. The bottom right frame of Figure 8 shows an event in which a purely adiabatic ET from the wet-electron state to a surface state is accompanied by a NA transfer from the surface state to another state with more localization on the H/H_2O ML. The individual ET events shown in Figure 8 represent examples of the electron injection scenarios that can be detected by single-molecule spectroscopies in the future. They show that at the single-molecule level, the transfer of the wet-electron can proceed by a broad range of scenarios. The variety of the ET scenarios is entirely hidden in the ensemble average data, Figure 7. Despite this large variation in the individual events, the average behavior of the system is quite straightforward. The wet-electron relaxation into the TiO_2 surface is very fast and has equal adiabatic and NA character, Figure 7.

3.5. Comparison of the Wet-Electron and Chromophore−Semiconductor Systems. The photoinduced ET in the chromophore−TiO_2 and H_2O−TiO_2 systems exhibits a number of similarities. This is particularly true if the chromophore is bound to the TiO_2 surface directly, without an intervening bridge.[22,74] In both types of systems, the ET is ultrafast and proceeds by a combination of adiabatic and NA ET mechanisms. The ET is driven by relatively slow vibrational modes. They are capable of generating fast injection due to a high density of electron acceptor states that can be accessed with minor atomic displacements by the adiabatic mechanism. Thermal atomic motions create a broad inhomogeneous distribution of initial conditions and a variety of injection scenarios. Ensemble measurements mask this variety and produce simple time-dependence of the ET process that can be well fitted by an exponential function. Further features of the experimental measurements of the ET processes in the wet-electron and chromophore−semiconductor systems may be uncovered with an explicit modeling of the

(74) Prezhdo, O. V.; Duncan, W. R.; Prezhdo, V. V. *Prog. Surf. Sci.* **2009**, *84*, 30.
(75) Hendry, E.; Wang, F.; Shan, J.; Heinz, T. F.; Bonn, M. *Phys. Rev. B* **2004**, *69*, 081101.

interaction with the optical laser fields. In particular, finite duration laser pulses can prepare photoexcited states that are not eigenstates of the electronic Hamiltonian for fixed atomic positions. Such electronic wavepackets can rapidly evolve purely due to quantum coherence effects even when the atoms are not moving. One can expect that in photovoltaic devices subjected to continuous-wave light such effects will be minor. Ultimately, in both systems, the injected electrons interact with the TiO_2 lattice and form polaron, as evidenced by THz spectroscopy.[75]

The differences between the properties of TiO_2 covered with chromophore and water layers arise from the true two-dimensional nature of the wet-electron state, as compared to the localized chromophore state. The wet-electron state is more strongly coupled to TiO_2 than are any of the molecular states, because the majority of the water atoms directly interact with TiO_2. In contrast, even in the smallest chromophores, the excited state wave function is localized away from the surface. As a result, the wet-electron state is much more delocalized into the semiconductor than are molecular states. The wet-electron is a true interfacial species that cannot exist separately in TiO_2 or water. Although the chromophore and semiconductor states do mix, generally the ET in the chromophore−semiconductor systems proceeds between distinct chromophore and surface states. The wet-electron is strongly coupled to the hydrogen atoms and may result in PCET,[67−72] complicating the wet-electron dynamics and requiring quantum-mechanical description of the atomic motion. Chromophore−semiconductor ET typically does not involve large-scale atomic rearrangements.

Time-resolved studies of wet-electrons provide a fundamental understanding of the role of the solvent in dye-sensitized semiconductor solar cells (DSSC).[2,3,22,74] The wet-electron state is higher in energy than the excited states of the majority of the chromophores used in DSSC. Therefore, pristine wet-electron states are not directly involved in the photovoltaic processes. However, solvents and electrolytes do play critical roles in the photovoltaic devices. Solvent molecules saturate the dangling bonds of the TiO_2 surface and strongly shift the energy levels of the charged species generated during ET. The energy of the reduced and oxidized states of the $I^{-}{}^{-}/I_3^{-}{}^{-}$ electrolyte that is most common in DSSC cannot be accurately obtained without considering the solvent. If electrolyte molecules are allowed to approach the TiO_2 surface, they can replace the solvent molecules saturating the surface dangling bonds, bind to TiO_2, and induce rapid electron loss. Following the characterization of the pristine wet-electron systems, one can envision similar studies of wet-electron states in the presence of a low concentration of electrolyte. Investigation of solvent layers deposited on TiO_2 surfaces that are already sensitized with dyes or contain a controlled concentration of defects can greatly advance the fundamental aspects of DSSC. Such studies can elucidate the importance and strength of the coupling of the solvent to the surface, chromophore, and electrolyte species, and establish the mechanisms of electron losses that limit the DSSC efficiencies.

4. Conclusions

The wet-electron state is a novel state whose characterization is crucial for the complete understanding of ET processes that occur at solid−liquid and molecule−bulk interfaces. Strong interfacial coupling favors delocalization of wet-electron states over both water and TiO_2. Wet-electrons cannot exist separately in either water or TiO_2. Similar states are present in a number of other systems, including dye-sensitized semiconductors and metal−liquid interfaces. These states share a number of common features, including short lifetime and little dependence on system details, such as defects and temperature.

The ab initio NAMD study of the wet-electron state as it exists on the $H/H_2O/TiO_2$ (110) surface has provided a detailed understanding of the ET dynamics of the system. The static electronic structure calculations performed previously[55,56] provided vital information in showing the dependence of the energy of the wet-electron state on the number of dangling H atoms present and their arrangement. The dynamic calculations reported here support the conclusions obtained in the time-independent studies and take one step further. The simulations directly mimic the experimentally observed time-resolved ET process and establish the mechanisms responsible for the movement of charge through the system. Finite temperature simulations have shown that atomic motion has an effect on both geometric and electronic structure of the wet-electron system. These thermal fluctuations cause changes in the orientations of the atoms, which in turn result in modifications of the energy and localization of the wet-electron state. The most significant contributions to the evolution of the wet-electron state energy and localization during the dynamics run are low frequency vibrational modes. These modes correspond to bending, torsional, and librational (hindered rotational) motions. Despite the large role played by these slow vibrations, ET occurs on the ultrafast time scale. The low frequency modes can still bring the wet-electron state to an energetic crossing point with the TiO_2 CB states very quickly, because the density of the TiO_2 acceptor states is high. Combined with the strong coupling between the surface and the adsorbant, repeated state crossings result in ultrafast ET.

Our group's implementation of NAMD has allowed for the determination of the ET mechanism in the wet-electron system. The ET process has almost equal contributions from both the adiabatic and the NA pathways. Initially, near 60% of the wet-electron state is localized on the TiO_2 substrate, thus showing strong donor−acceptor coupling. The transfer process occurs in less than 10 fs. Thermal motions of the system produce an inhomogeneous ensemble of initial conditions from which ET can occur. Some of these individual events are dominated by adiabatic ET, while others are mostly NA. Also, some ET processes are straightforward, while others show multiple steps and great complexity. All events lead to fast ET. The simulation shows distinct wet-electron, surface, and bulk states, indicating that the wet-electron transfers first into TiO_2 surface and then bulk. The wet-electron and related states play key roles in many interfacial ET processes involved in a wide variety of applications. The simulation of the wet-electron dynamics provides insights that are valuable for catalysis, electrolysis, photovoltaics, photo-, and electrochemistry.

Acknowledgment. We are grateful to Hrvoje Petek and Ken Jordan for many valuable discussions. This research was supported by grants from NSF CHE-0701517 and ACS PRF 41436-AC6.

JA906599B